NANO LETTERS

2006
Vol. 6, No. 10
2254−2259

Complex Buckling Instability Patterns of Nanomembranes with Encapsulated Gold Nanoparticle Arrays

Chaoyang Jiang,[†,‡] Srikanth Singamaneni,[†,‡] Emily Merrick,[†] and Vladimir V. Tsukruk*[,†,‡]

Department of Materials Science and Engineering, Iowa State University, Ames, Iowa 50011, and School of Materials Science and Engineering, Georgia Institute of Technology, Atlanta, Georgia 30332

Received July 15, 2006; Revised Manuscript Received August 22, 2006

ABSTRACT

The nanomechanical properties of micropatterned nanomembranes containing gold nanoparticle microarrays were investigated with the buckling instability method. An unusual, complex pattern of buckling instability was observed for the nanoscale polymeric films under compressive stresses. An intriguing two-stage wrinkling was observed for these nanoscale films with spatially correlated instabilities. Two concurrent strain-dependent buckling modes were observed above a certain critical strain. Transformation from conventional transversal buckling mode to zigzag buckling is attributed to the development of the biaxial stress along the boundary lines for micropatterned areas. The binary buckling pattern observed here allowed the "one-shot" evaluation of the elastic moduli of two compositionally different regions (with and without gold nanoparticles).

Micromechanical instabilities of nanoscale polymeric films under stresses (mechanical or thermal) resulting in the formation of spontaneous regular buckling patterns (wrinkling) is considered to be important for both measuring nanoscale mechanical properties and as a nonlithography route for microscopic patterning. Thermodynamically driven to minimize the elastic strain energy, this Euler-type instability has been known for many years and is frequently found in nature (e.g., aging human skin).[1] However, recent buckling instability patterns guided by predesigned substrates can be highly ordered and strikingly uniform at different length scales with diversity in shape and size.[2−4] Tunable optical gratings, waveguide structures, thermal and acoustic microsensors, and microfluidic arrays can be thought of as prospective applications.[5−10] The vast majority of research conducted to date has been limited to thin metal films on elastic substrates or surface-treated elastomers. Very few studies have focused on buckling phenomena of uniform ultrathin polymer films[11] and nanoscale films such as layer-by-layer (LbL) films.[12]

In this letter, we report the nanomechanical properties of two-phase nanoscale LbL films with gold nanoparticles encapsulated into multilayered LbL films in a patterned manner (Figure 1). Two *strain-dependent buckling modes* (binary buckling) were observed under compressive strain. Above first critical strain, the transversal buckling of stiffer regions was observed, and exceeding second critical strain resulted in zigzag buckling across stiff and compliant regions. Reorientation of wrinkles accompanying this transformation is attributed to the development of the biaxial stress due to nontangential orientation of compressive stresses in the vicinity of the boundary lines and significant shear stresses caused by mismatch in the regional compliances.

Nanoscale LbL films with precise subnanometer control over the assembly of various functionalized blocks are of increasing interest because of prospective applications in modern micro- and nanodevices.[13−19] The nanoscale LbL films studied here are prepared with LbL assembly, which involves alternating adsorption of oppositely charged functional blocks.[20−22] LbL films of encapsulated gold nanoparticles (13 nm diameter)[23] in poly(allylamine hydrochloride) (PAH) and poly(sodium 4-styrenesulfonate) (PSS) matrix, with a formula $(PAH/PSS)_9PAH/Au/(PAH/PSS)_9PAH$ (designated below as 9G*9), were fabricated with spin-assisted LbL assembly combined with microprinting.[24,25] The free-standing LbL films were transferred to a PDMS substrate and compressed by 0.1−0.5% (compressive stresses 2−10 kPa). Finite element analysis (FEA) was used to estimate the stress distribution with COMSOL Multiphysics 3.2.

The atomic force microscopy (AFM) image shows the two-phase microstructure of the LbL film with alternating

* To whom correspondence should be addressed. E-mail: vladimir@mse.gatech.edu.
† Iowa State University.
‡ Georgia Institute of Technology.

10.1021/nl061630n CCC: $33.50
Published on Web 09/08/2006

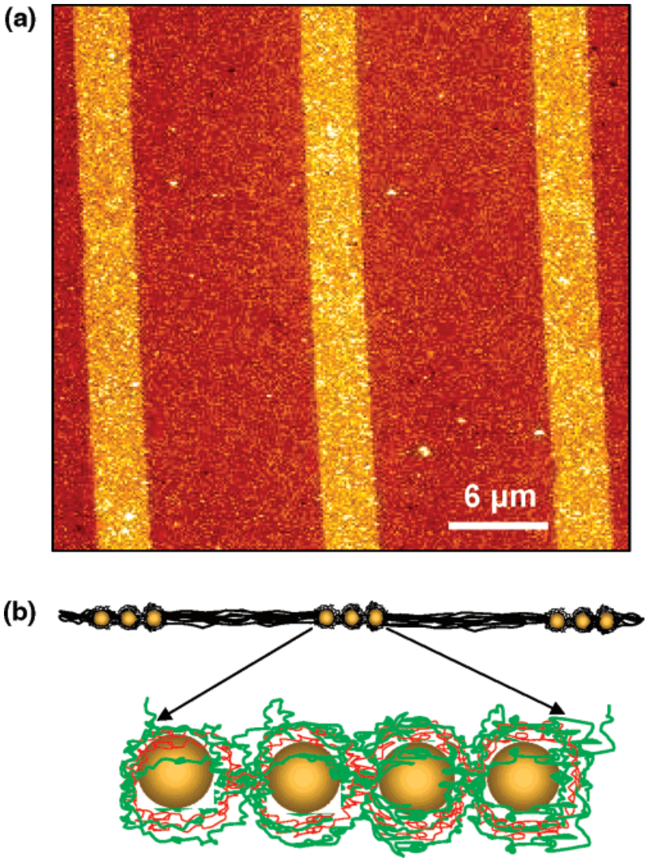

Figure 1. (a) AFM image of 9G*9 LbL film showing the vertical regions of encapsulated gold nanoparticles (brighter stripes) alternating with all-polymeric LbL regions. The schematic (b) represents the side-view of the LbL film in the free-standing state with patterned gold nanoparticles and a corresponding close view (bottom, ref 17).

regions of polyelectrolyte multilayers without (54 nm thick) and with (60 nm thick) gold nanoparticles (Figure 1). The stripes (3 μm wide) reinforced with gold nanoparticles ($\sim$4 volume %) are separated by 7-μm-wide regions, making the overall periodicity 10 μm (for a detailed discussion of LbL microstructure see ref 17). The hypothesis in this study was that the presence/absence of gold nanoparticles in the selected regions resulting in different elastic properties could affect their buckling behavior, leading to complex buckling of the instability pattern. In fact, a gentle compression ($\sim$0.2% strain) of the LbL film along stripes resulted in immediate appearance of peculiar transversal periodic buckling patterns *strictly* confined to stiffer gold-containing regions with very few of them extending across all-polymeric regions, as observed in both optical micrographs and AFM images. Three representative images are shown in Figure 2, and more selected experimental results for different surface locations and different magnifications are provided in the Supporting Information. AFM images demonstrate that these wrinkles indeed represent modulated surface topography with amplitude of 80 nm (Figure 2b and c). Spacing of these wrinkles determined from optical micrographs was 2.9 $\pm$ 0.3 μm, which is consistent with that obtained from AFM images (see below). The spacing quoted here was obtained from 1D and 2D FFT data, which provide the parameters averaged over a whole image and typically includes about a hundred wrinkles. Therefore, the overall analysis performed here included about 1000 wrinkles.

As demonstrated in large-scale optical images, although about 80% of the film surface shows uniform buckling behavior, the film deformation also involves the formation of flat regions and microcracks running parallel to the strain direction (see Figure 2a and the Supporting Information). The appearance of these defects is related to both local delamination of the film and other modes of stress release.[7] A closer inspection of AFM images reveals that the amplitude of the buckling pattern is considerably different in certain regions, which is related to the localized stress distribution due to the variable adhesion and delamination, especially near the cracks and other defect areas. However, because the periodicity of these buckling patterns is independent of the amplitude as far as the local stress is higher than the critical stress, in our experiments we measure only threshold stress, which is independent of compression.

Further compression of the LbL films above 0.3% strain resulted in a sudden transformation of the initial buckling pattern with the reorientation of the initial transversal buckling and the formation of the new skewed wrinkles between gold-containing stripes (Figure 2d and Supporting Information). These buckling patterns with zigzag wrinkles expanded over many alternating regions (Figure 2d). The inset in Figure 2d (14 $\times$ 14 μm^2) provides a closer look at the boundary line, revealing not only clearly different periodicity but also a bend occurring at the boundary line. Finally, at even higher strains exceeding 1% a network of microcracks was formed[26] (see the Supporting Information).

Data analysis with more than 10 optical images, with different samples and surface locations, were conducted and the typical results of the analysis of these complex buckling patterns with 2D Fourier transforms (FT) demonstrates three distinctive Fourier components related to the overall periodicity of the micropattern (d = 10 μm) along with the smeared close spots at much larger wavenumbers (Figure 2e). These two other components correspond to the buckling modes with different periodicities λ_1 and λ_2, arranged at an angle β to the boundary normal (39°) and with an angle α ($\sim$5°) between them. To obtain precise values of corresponding periodicities, we analyzed cross-sectional profiles along several principal directions of the buckling pattern (Figure 3). Profile 3a describes primary spacing caused by a micropattern, which reveals itself in a strong peak on 1D FT at 10 μm (Figure 3a). Corresponding sections along two other buckling modes generate periodic profiles and sharp 1D Fourier peaks, which give the wrinkle periodicity λ_1 = 2.1 $\pm$ 0.2 μm (as calculated after correction on optical doubling) for the regions without gold nanoparticles and λ_2 = 2.9 $\pm$ 0.3 μm for the regions with gold nanoparticles (which is close to that obtained from independent AFM measurements (Figure 3b and c).

This complex nature of the binary buckling pattern and its transformation under increasing stress observed here can be understood considering the buckling phenomena for stiffer films deposited on a more compliant substrate. Periodic

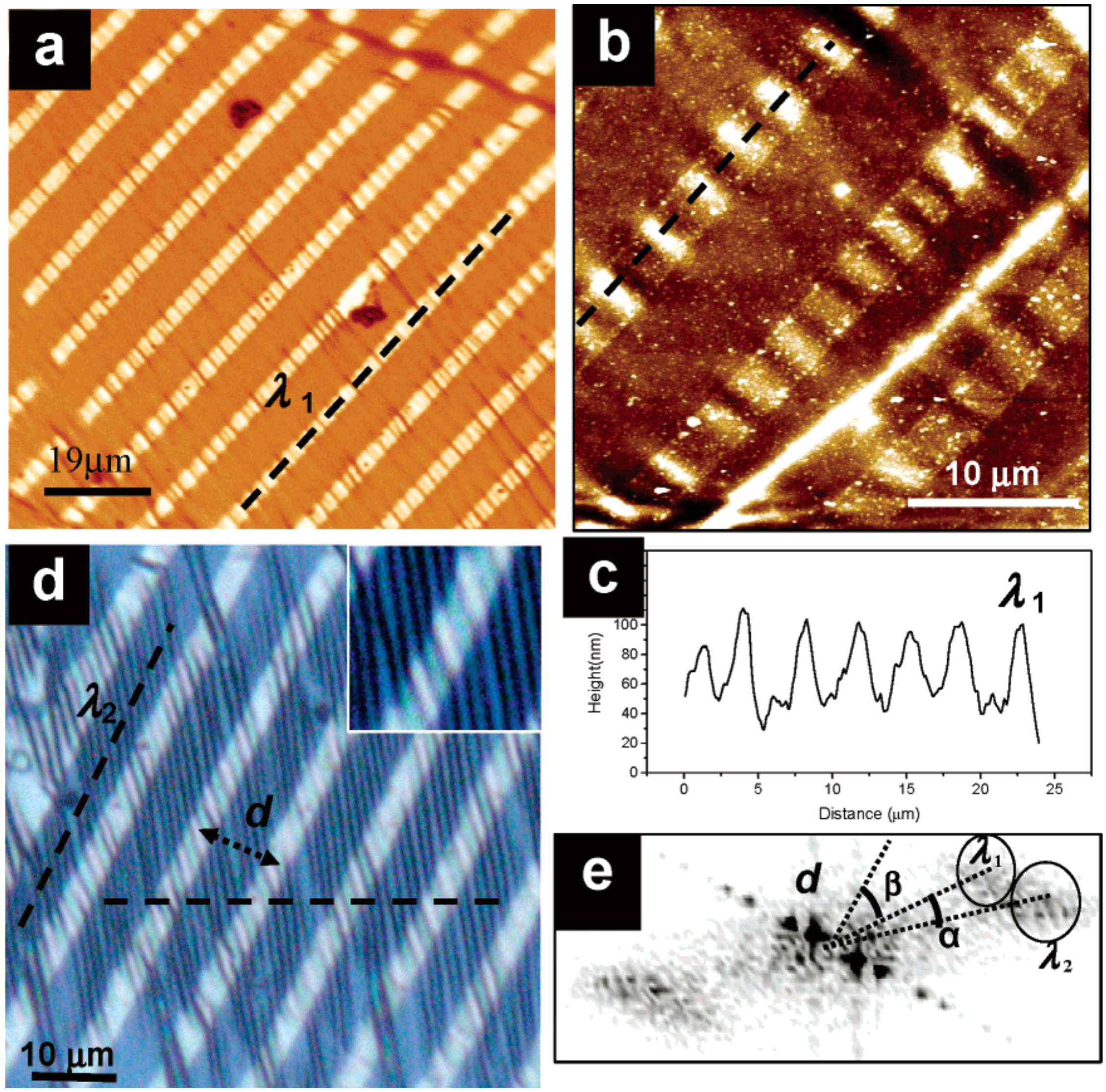

Figure 2. Buckling patterns of micropatterned LbL film: (a and b) one-dimensional buckling mode at low strain (about 0.2%), optical (a) and AFM (b) images. (c) Height profile of buckling mode (dashed line in part b). (d) Binary buckling pattern at higher compression strain (>0.3%); the inset is a 14×14 μm^2 image showing the close look at the boundary line. (e) 2D FT of the buckling pattern (a) with three distinct Fourier components. The dashed lines show corresponding cross sections demonstrated in Figure 3.

buckling patterns are formed spontaneously to minimize the strain energy at compressive stress above a certain threshold (Figure 4).[1,27] The buckling occurs with a characteristic periodicity, λ, determined by the mechanical properties of the substrate and the film as

$$\lambda = 2\pi t\left[\frac{(1-\nu_s^2)E_f}{3(1-\nu_f^2)E_s}\right]^{1/3} \tag{1}$$

where E and υ are the elastic modulus and the Poisson's ratio for film and substrate (f and s), respectively, and t is the thickness of the film. The amplitude of the buckling mode, A, depends on compressive strain induced as[1]

$$A \sim \lambda\sqrt{\epsilon} \tag{2}$$

Finally, the critical strain for impending buckling instability, ϵ_c, is determined by the ratio of elastic moduli[26]

$$\epsilon_c = -\frac{1}{4}\left(\frac{3E_s(1-\upsilon_f^2)}{E_f\,(1-\upsilon_s^2)}\right)^{2/3} \tag{3}$$

General conditions for the buckling instability presented by eqs 1−3 suggest that the coexisting wrinkles with different periodicities are caused by different elastic properties of regions with lower (without gold nanoparticles) and higher (encapsulated gold nanoparticles) elastic moduli (Figure 4). In fact, if the Poisson's ratio is not altered significantly by the presence of nanoparticles, then the buckling periodicity should simply scale with the localized elastic modulus: $\lambda \sim tE_f^{1/3}$. The nanoparticle reinforcement in selected regions of the LbL film increases the elastic modulus by 2- to 3-fold,[17] and such an increase should result in a significant (50%) increase in the buckling periodicity (eq 1) (neglecting 10% difference in thicknesses). Moreover, a significant

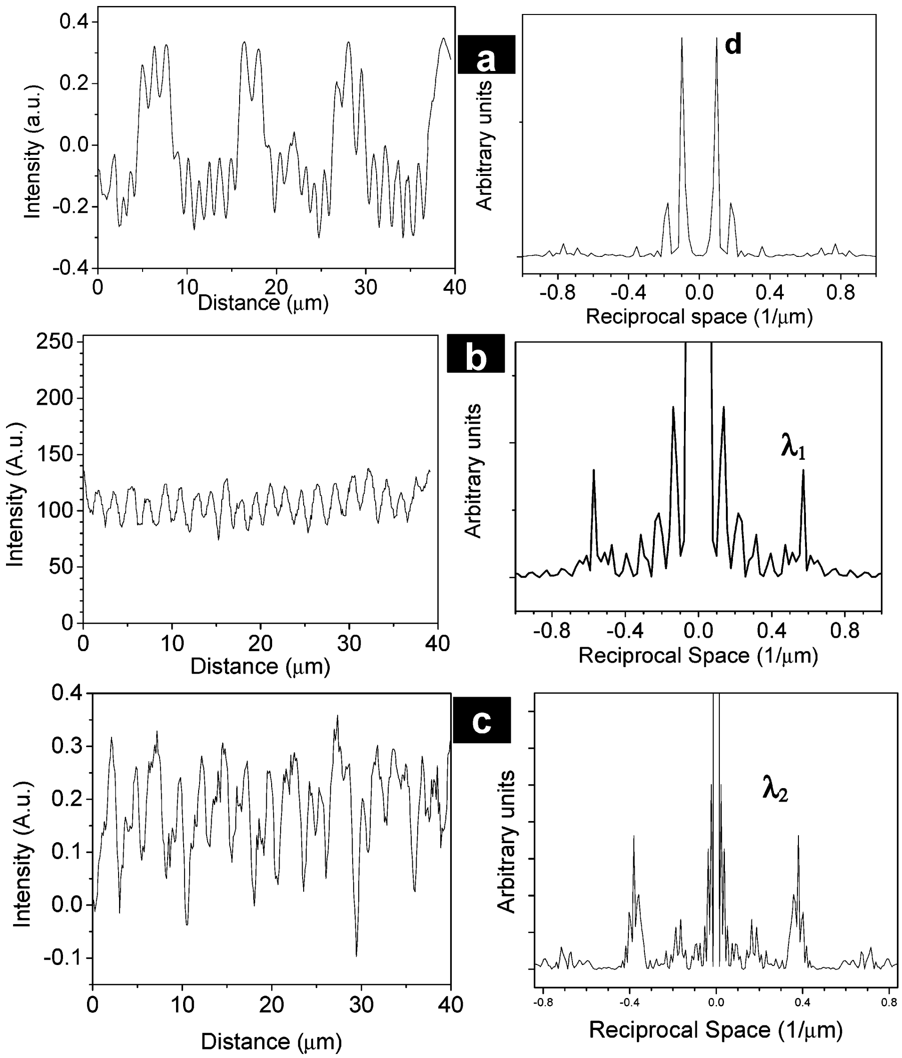

Figure 3. Cross-sectional profiles (left) and corresponding 1D FT plots (right) for different buckling patterns. The locations of the sections are marked in optical image shown in Figure 2a and c with dashed lines.

decrease in the critical strain is expected for regions reinforced with gold nanoparticles. Estimation of theoretical threshold strains for two different regions from eq 3 gives values $\epsilon_{c1} = 0.18\%$ and $\epsilon_{c2} = 0.24\%$ for nanoparticle-containing and purely polymeric regions, respectively.

Therefore, for micropatterned LbL films designed here with different elastic moduli of purely polymeric and nanoparticle-reinforced regions, we can suggest that the gradual compression should result in *two* strain-dependent instabilities, strikingly different from uniform polymer films studied earlier. Exceeding lower critical strain for stiffer regions, ϵ_{c1}, results in first buckling instability mode generated with λ_1, whereas more compliant regions remain in a planar state (Figure 4b). Further compression to strain above ϵ_{c2} generates a second buckling mode in more compliant regions with a smaller periodicity, λ_2 (Figure 4b). The experimentally observed transformations within 0.2−0.3% strain range correspond closely to theoretical estimations (within experimental accuracy). Estimation of the elastic properties of two different regions from eq 1 gives $E_1 = 3.0 \pm 0.7$ GPa and $E_2 = 1.6 \pm 0.3$ GPa; both values are in good agreement with independently measured elastic modulus of the nanoparticle-containing LbL film (4−6 GPa) and the polymer PSS−PAH film (1−2 GPa).[28] Moreover, the composite elastic modulus calculated from these values assuming isostrain conditions is about 2.0 GPa, which corresponds exactly to the actual modulus of 2.1 GPa as measured independently from the bulging test. In addition, the amplitude of the buckling pattern (A) within 80−100 nm is fairly close to the theoretical estimation (100−200 nm from eq 2).

The other interesting aspect of the observed binary buckling phenomenon is the reorientation of the buckling patterns after second transition, which manifests itself in realignment of wrinkles within two regions at angles $\beta_1 = 39°$ and $\beta_2 = 34°$ (Figure 2e). This unusual behavior demonstrates significant coupling between the two buckling modes and complex stress distribution. To clarify this behavior, we modeled stress distribution within a two-phase film with FEA. [In Figure 4c, the elastic modulus mismatch was intentionally chosen to be high (8 times difference instead of 2) in order to visualize the stress distribution.] We observed a complex distribution of compressive stresses within a more compliant region with a deviation of the local

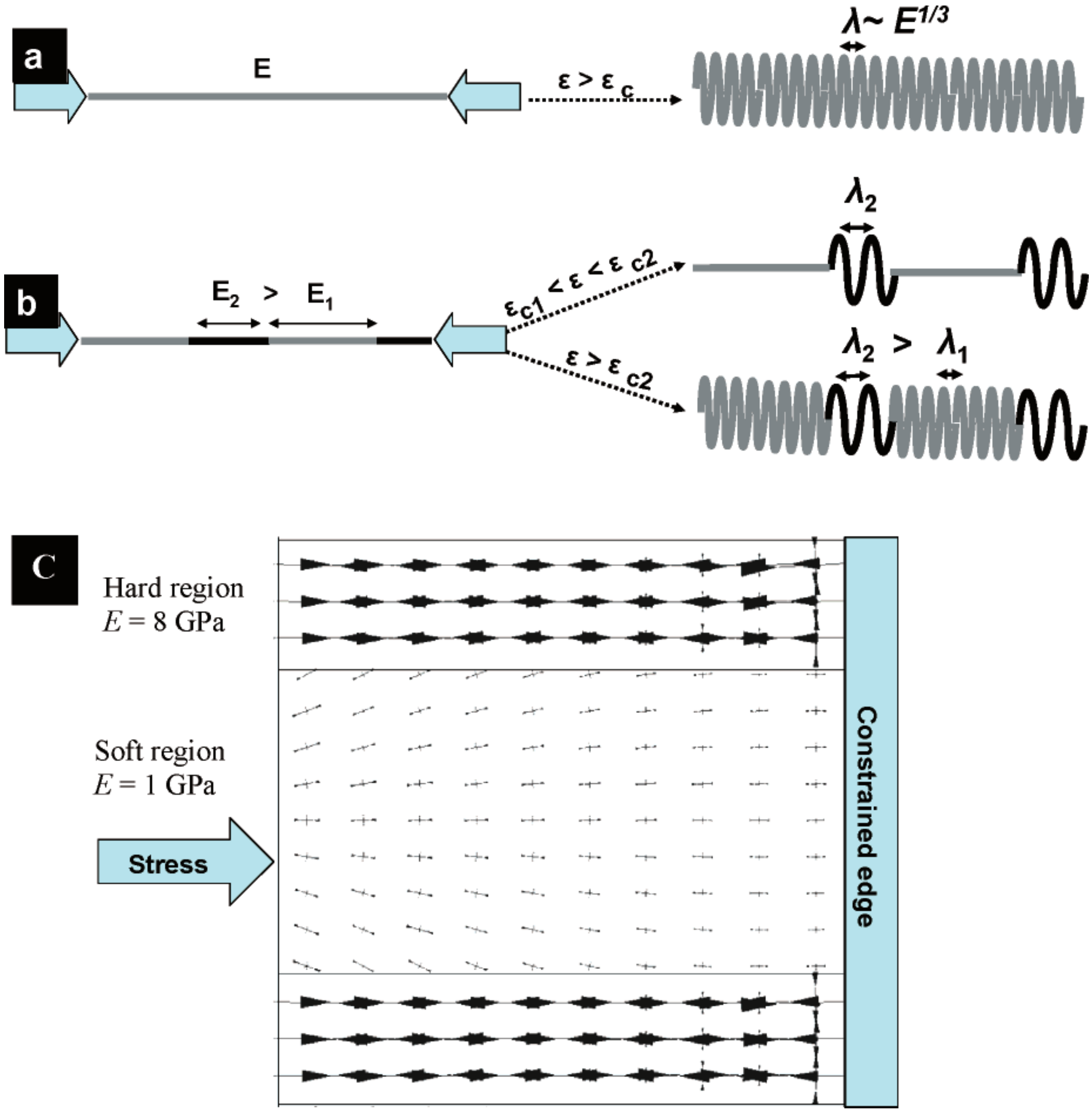

Figure 4. Different buckling scenarios: (a) a single buckling mode in uniform films under compressive stress; (b) binary buckling occurring at different critical stresses in two-phase film. (c) 2D stress distribution from FEA modeling of two-phase film composed of domains with different elastic moduli demonstrating mismatch along the boundary lines.

director from the longitudinal direction (up to 5° for actual elastic parameters) in the vicinity of the boundary lines. Even more important is a significant difference in the absolute values of stresses developed within less and more compliant regions under isostrain conditions (Figure 4c). This difference causes shear stresses along the boundary lines not accounted for in the simple model of the buckling instability. Thus, we suggest that under the high shear stress the variation of stress field along the boundary line creates a biaxial stress distribution and causes spontaneous reorientation of the wrinkles to realign the direction to the maximum local stress. Bending of the wrinkles occurring at the boundary (5°) can be related to additional stresses associated with the mismatch of incommensurated periodicities at the boundary line. The resulting zigzag pattern reminds us of a stretched version of the herringbone pattern suggested as an effective way to relax biaxial stresses.[29]

Simultaneous measurement of micromechanical properties of different microscopic regions within two-phase nanoscale polymeric films from the binary buckling pattern can be suggested as an intriguing metrology tool for rapid evaluation of local, phase-specific micromechanical properties inaccessible with usual methods. The method has unique advantages over other techniques, which include rapid screening, localized measurement, relative robustness and simplicity in concurrent obtaining and processing the experimental data, and sensitive to chemical composition of the microscopic regions of multiphase materials.

In conclusion, we demonstrate strain-dependent formation of the *binary buckling patterns* for specially designed two-phase micropatterned nanoscale LbL films with alternating regions of different elastic properties caused by the encapsulation of the micropatterned array of gold nanoparticles. The complex wrinkle patterns observed here were caused by the variation of the stress field along the boundary line due to the different mechanical properties of components in the nanocomposite thin film. We suggest that the induction of a specific buckling pattern via imprinting an array of nanoparticles into nanoscale polymeric films can be expanded toward much more complex multiscale wrinkles.

Acknowledgment. We thank M. C. LeMieux, M. Ornatska, and M. E. McConney for technical assistance and invaluable help. PDMS substrate was generously provided by A. Nolte, MIT. This work is supported by AFOSR, FA9550-05-1-0209 and NSF-NIRT-0506832 Grants.

Supporting Information Available: Additional optical and AFM images. This material is available free of charge via the Internet at http://pubs.acs.org.

References

(1) Genzer, J.; Groenewold, J. *Soft Matter* **2006**, *2*, 310−323.
(2) Bowden, N.; Brittain, S.; Evans, A. G.; Hutchinson, J. W.; Whitesides G. M. *Nature* **1998**, *393*, 146−149.
(3) Mahadevan, L.; Rica, S. *Science* **2005**, *307*, 1740.
(4) Moon, M. W.; Lee, K. R.; Oh K. H.; Hutchinson J. W. *Acta Mater.* **2004**, *52*, 3151−3159.
(5) Hiller, J.; Mendelsohn, J. D.; Rubner, M. F. *Nat. Mater.* **2002**, *1*, 59−63.
(6) Edmondson, S.; Frieda, K.; Comrie, J. E.; Onck, P. R.; Huck, W. T. S. *Adv. Mater.* **2006**, *18*, 724−728.
(7) Efimenko, K.; Rackaitis, M.; Manias, E.; Vaziri, A.; Mahadevan L.; Genzer, J. *Nat. Mater.* **2005**, *4*, 293−297.
(8) Huang, R. *Appl. Phys. Lett.* **2005**, *87*, 151911.
(9) Cerda, E.; Mahadevan, L. *Phys. Rev. Lett.* **2003**, *90*, 074302.
(10) Harrison, C.; Stafford, C. M.; Zhang, W.; Karim, A. *Appl. Phys. Lett.* **2004**, *85*, 4016−4018.
(11) Stafford, C. M.; Harrison, C.; Beers, K. L.; Karim, A.; Amis, E. J.; Vanlandingham, M. R.; Kim, H.; Volksen, W.; Miller R. D.; Simonyi E. E. *Nat. Mater.* **2004**, *3*, 545−550.
(12) Nolte, A. J.; Rubner, M. F.; Cohen, R. E. *Macromolecules* **2005**, *38*, 5367−5370.
(13) Haynie, D. T.; Zhang, L.; Rudra, J. S.; Zhao, W.; Zhong, Y.; Palath, N. *Biomacromolecules* **2005**, *6*, 2895−2913.
(14) Granick, S.; Kumar, S. K.; Amis, E. J.; Antonietti, M.; Balazs, A. C.; Chakraborty, A. K.; Grest, G. S.; Hawker, C.; Janmey, P.; Kramer, E. J.; Nuzzo, R.; Russell, T. P.; Safinya, C. R. *J. Polym. Sci., Part B: Polym. Phys.* **2003**, *41*, 2755−2793.
(15) Jiang, C.; Lio, W. Y.; Tsukruk, V. V. *Phys. Rev. Lett.* **2005**, *95*, 115503.
(16) *Multilayer Thin Films*; Decher, G., Schlenoff, J. B., Eds.; Wiley-VCH: Weiheim, Germany, 2003.
(17) (a) Jiang, C.; Markutsya, S.; Pikus, Y.; Tsukruk, V. V. *Nat. Mater.* **2004**, *3*, 721−728. (b) Jiang, C.; Markutsya, S.; Tsukruk, V. V. *Adv. Mater.* **2004**, *16*, 157−161. (c) Jiang, C.; Markutsya, S.; Tsukruk, V. V. *Langmuir* **2004**, *20*, 882−890.
(18) Jiang, C.; Tsukruk, V. V. *Adv. Mater.* **2006**, *18*, 829−840.
(19) Johnston, A. P. R.; Read, E. S.; Caruso, F. *Nano Lett.* **2005**, *5*, 953−956.
(20) Li, J.; Möhwald, H.; An, Z.; Lu, G. *Soft Matt.* **2005**, *1*, 259−264.
(21) Schneider, G.; Decher, G.; Nerambourg, N.; Praho, R.; Werts, M. H. V.; Blanchard-Desce, M. *Nano Lett.* **2006**, *6*, 530−536.
(22) Hammond, P. T. *Adv. Mater.* **2004**, *16*, 1271−1293.
(23) Jiang, C.; Markutsya, S.; Shulha, H.; Tsukruk, V. V. *Adv. Mater.* **2005**, *17*, 1669−1673.
(24) Shchukin, D. G.; Kommireddy, D. S.; Zhao, Y.; Cui, T.; Sukhorukov, G. B.; Lvov, Y. M. *Adv. Mater.* **2004**, *16*, 389−393.
(25) Tsukruk, V. V. Ko, H.; Peleshanko, S. *Phys. Rev. Lett.* **2004**, *92*, 065502.
(26) Volynskii, A. L.; Bazhenov, S.; Lebedeva, O. V.; Bakeev, N. F. *J. Mater. Sci*. **2000**, *35*, 547−554.
(27) Groenewold, J. *Physica A* **2001**, *298*, 32−45.
(28) Jiang, C.; Kommireddy, D. S.; Tsukruk, V. V. *Adv. Funct. Mater.* **2006**, *16*, *27*-32.
(29) Chen, X.; Hutchinson, J. W. *J. Appl. Mech. Trans. ASME* **2004**, *71*, 597−603.

NL061630N